

Pressure-Regulated Dynamic Stereochemical Role of Lone-Pair Electrons in Layered $\text{Bi}_2\text{O}_2\text{S}$

Kejun Bu, Hui Luo, Songhao Guo, Mei Li, Dong Wang, Hongliang Dong, Yang Ding, Wenge Yang, and Xujie Lü*

Cite This: *J. Phys. Chem. Lett.* 2020, 11, 9702–9707

Read Online

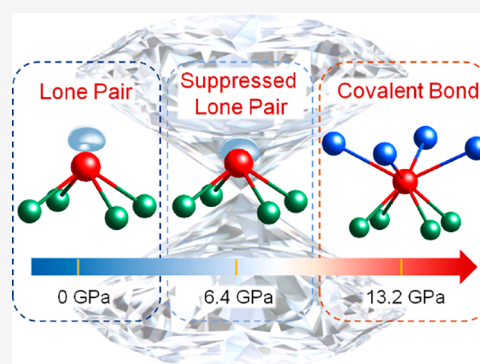
ACCESS |

Metrics & More

Article Recommendations

Supporting Information

ABSTRACT: Lone-pair electrons (LPEs) ns^2 in subvalent 14 and 15 groups lead to highly anharmonic lattice and strong distortion polarization, which are responsible for the groups' outstanding thermoelectric and optoelectronic properties. However, their dynamic stereochemical role in structural and physical properties is still unclear. Here, by introducing pressure to tune the behavior of LPEs, we systematically investigate the lone-pair stereochemical role in a $\text{Bi}_2\text{O}_2\text{S}$. The gradually suppressed LPEs during compression show a nonlinear repulsive electrostatic force, resulting in two anisotropic structural transitions. An orthorhombic-to-tetragonal phase transition happens at 6.4 GPa, caused by the dynamic cation centering. This structural transformation effectively modulates the optoelectronic properties. Further compression beyond 13.2 GPa induces a 2D-to-3D structural transition due to the disappearance of the Bi- $6s^2$ LPEs. Therefore, the pressure-induced LPE reconfiguration dominates these anomalous variations of lattice, electronic, and optical properties. Our findings provide new insights into the materials optimization by regulating the characters of LPEs.



Two-dimensional (2D) bismuth-based materials possessing unique physical and chemical properties have shown great promise for energy conversion and storage applications.^{1–3} Since the first discovery of BiOX ($X = \text{Cl}, \text{Br}, \text{I}$) in photocatalysis in 2006,⁴ the derivative compounds have exhibited ample functionalities including optoelectronic $\text{Bi}_2\text{O}_2\text{S}$,⁵ thermoelectric BiOCuSe , and nonlinear optical $\text{BiO}(\text{IO}_3)$.⁶ The key aspect regarding the origins of their remarkable functionalities is to understand the effects of the Bi- $6s^2$ lone pair electrons (LPEs) on their atomic and electronic structures.^{7,8} The heavy p-block Bi shows far-dispersed $6s^2$ valence orbitals involved in constructing the valence band maximum (VBM) near the Fermi surface, which greatly affects the electronic structures and physical properties.⁹ Moreover, the nonlinear repulsive electrostatic force, as influenced by the stereochemical Bi- $6s^2$ LPEs, leads to a distorted lattice, weak bonding, and large interlayer space.^{5,10,11} Such unique electronic structure and lattice distortion give rise to high phonon anharmonicity and strong distortion polarization, which thus effectively contribute to low thermal conductivity in thermoelectric materials and high photoresponse in optoelectronic materials.^{7,11–13}

Despite the great significance of LPEs in these functional materials, an understanding of the dynamic stereochemical role of LPEs is still very lacking. It is also unclear how to modify the configuration of LPEs toward high performance. Recently, the temperature-dependent behavior of LPEs was reported in halide perovskite CsSnBr_3 , where the displacement of LPEs

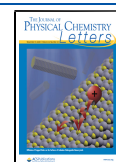
causes the emergence of the lattice expansion and Sn^{2+} off-centering in the octahedra.¹⁴ However, since the temperature control is relatively limited by the thermal stability of materials, the role of the dynamic stereochemistry of LPEs on the local structures, physical properties, and electronic structures remains unclear. As an alternative thermodynamic parameter, pressure provides a clean and effective means to adjust the atomic and electronic structures by changing the bond distances,^{15–18} and thus, the characters of LPEs can be modified. Therefore, we applied external pressure to carefully regulate the behaviors of LPEs and *in situ* monitored the variations of structures and properties, which would further our fundamental understanding and discover more emergent phenomena.

In this work, we selected an oxychalcogenide $\text{Bi}_2\text{O}_2\text{S}$ as an exemplar to articulate the stereochemical role of LPEs on the lattice, electronic structures, and physical properties. In comparison with other 2D bismuth-based materials, $\text{Bi}_2\text{O}_2\text{S}$ possesses a loose structure and strong LPE-induced lattice distortion, as well as a suitable bandgap of ~ 1.6 eV and rapid

Received: September 22, 2020

Accepted: October 26, 2020

Published: November 2, 2020



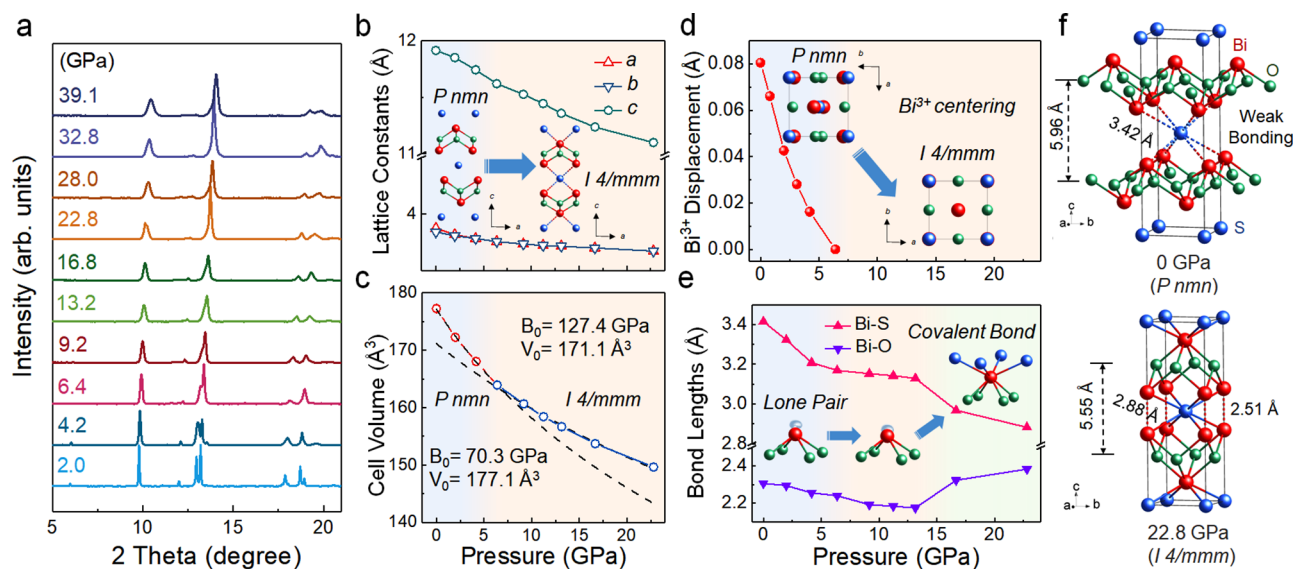


Figure 1. Structural characterization of $\text{Bi}_2\text{O}_2\text{S}$ with *in situ* synchrotron diffractions. (a) XRD patterns of $\text{Bi}_2\text{O}_2\text{S}$ at selected pressures. Variations of (b) lattice constants and (c) unit-cell volume during compression. By fitting the Birch–Murnaghan equation of state, the values of bulk modulus B_0 were determined to be 70.3 and 127.4 GPa before and after the phase transition, respectively (details in the Supporting Information). (d) Evolution of Bi^{3+} off-centering displacement from the vertex of the BiS_4 square pyramid with increasing pressure. The displacement reaches zero at above 6.4 GPa caused by the phase transition from orthorhombic to tetragonal structure. The inset of the panel illustrates the structural difference between the two phases (along the ab plane). (e) Bond lengths of Bi–O and Bi–S as a function of pressure. The inset shows the dynamic stereochemical evolution of LPEs under high pressure, i.e., the dynamic cation centering accompanied by a weakening of phonon anharmonicity, the suppression of LPEs, and the disappearance of LPEs. (f) The crystal structures of $\text{Bi}_2\text{O}_2\text{S}$ at ambient pressure and at 22.8 GPa. The dashed line shows the nominal Bi···S bonds at ambient pressure.

photoresponse for potential optoelectronic applications.⁵ Our findings reveal that the strong repulsion of the stereochemically active LPEs during compression causes the weakening of phonon anharmonicity and dynamic Bi^{3+} centering, which results in an orthorhombic-to-tetragonal phase transition and significantly enhanced optoelectronic properties. The disappearance of the LPEs induces a 2D-to-3D structural transition under higher pressures. The pressure-regulated LPEs cause a series of anomalous variations of structural, electrical, and optical properties.

$\text{Bi}_2\text{O}_2\text{S}$ crystals in dark-red cuboid shape were synthesized by a solvothermal method. The pristine crystals were confirmed to have stoichiometric and uniform distribution of the elements via a scanning electron microscope with energy-dispersive X-ray mapping (Figure S1). $\text{Bi}_2\text{O}_2\text{S}$ possesses a primitive orthorhombic lattice with the space group $Pn\bar{m}n$ (no. 58) at ambient conditions ($a = 3.874(1)$ Å, $b = 3.840(5)$ Å, $c = 11.916(1)$ Å, and $V = 177.2(6)$ Å³). Unlike most 2D van der Waals semiconductors, the $[\text{Bi}_2\text{O}_2]^{2+}$ cationic layers sandwich S^{2-} anionic square arrays by weak electrostatic interactions, which are derived from the interlayer coupling of LPEs (Figure 1f).^{5,8,19} These stereochemical Bi-6s^2 LPEs cause strong anharmonicity and rattling of Bi^{3+} cations along the ab planes, which lead to the slip of the S lattices and the off-centering of Bi^{3+} cations.⁸ Thus, the crystallographic symmetry of $\text{Bi}_2\text{O}_2\text{S}$ is lower than those of isostructural $\text{Bi}_2\text{O}_2\text{X}$ ($X = \text{Se}, \text{Te}$) (space group $I4/m\bar{m}m$). By regulating the structural distortion, pressure could be an effective way to adjust the local structure and thus considerably change the stereochemical role of LPEs in $\text{Bi}_2\text{O}_2\text{S}$.

In situ synchrotron X-ray diffraction (XRD) measurements for $\text{Bi}_2\text{O}_2\text{S}$ were performed up to 40 GPa to reveal the structural variations and the dynamic stereochemical evolution of LPEs (Figure 1, Figure S2, and Table S3). The Rietveld

analysis profiles for representative powder XRD data are shown in Tables S1 and S2 and Figure S3. With the increase of pressure, some diffraction peaks disappeared at 6.4 GPa, indicating a pressure-induced phase transition toward a higher symmetry (Figure 1a). Through analysis of single-crystal XRD, an orthorhombic structure with the space group $Pn\bar{m}n$ was indexed below 6.4 GPa, while a tetragonal $I4/m\bar{m}m$ structure was indexed after the phase transition. It is interesting to note that the degree of Bi^{3+} off-centering displacement weakens during compression, which is due to the suppressed stereochemical activity of LPEs under pressure (Figure 1d). Hence, the orthorhombic-to-tetragonal transition mainly arises from the gradually suppressed LPEs during compression, which results in the weaker phonon anharmonicity and a more ordered lattice (Figure 1d inset). More detailed discussion about the suppressed phonon anharmonicity can be seen in the Supporting Information. With increasing pressure, the tetragonal phase can be maintained with broadening and weakening XRD peaks. Upon decompression, the phase transition is irreversible, as evidenced by the retaining of the high-pressure $I4/m\bar{m}m$ phase (Tables S1 and S2 and Figure S4).

The pressure-induced variations of the lattice parameters and unit-cell volume of $\text{Bi}_2\text{O}_2\text{S}$ are shown in Figures 1b and 1c and Table S1. The orthorhombic structure shows a large anisotropic compressibility where the lattice along the c axis shortens more rapidly than those along a and b directions (Figure 1b). The lattice parameters along the a and b axes gradually become equivalent during compression (Table S1), which indicates the transition from an orthorhombic phase to a tetragonal phase. Meanwhile, the distance of the Bi···S bond decreases more rapidly than that of the Bi–O bond below 6.4 GPa, followed by a gentle decreasing slope similar to that of the Bi–O bond up to 13.2 GPa (Figure 1e). This different

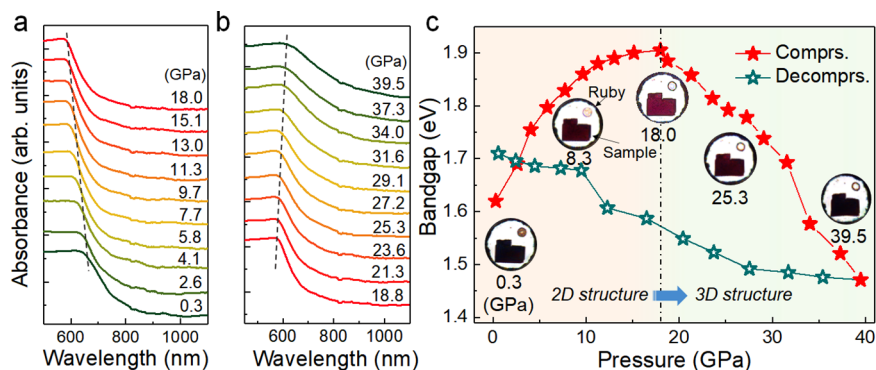


Figure 2. *In situ* optical measurements of $\text{Bi}_2\text{O}_2\text{S}$ under pressure. (a, b) Selective UV–vis absorption spectroscopy on a single-crystal $\text{Bi}_2\text{O}_2\text{S}$ under compression. (c) Bandgap evolution of the $\text{Bi}_2\text{O}_2\text{S}$ crystal under high pressure and the optical images at selected pressures during a compression–decompression cycle.

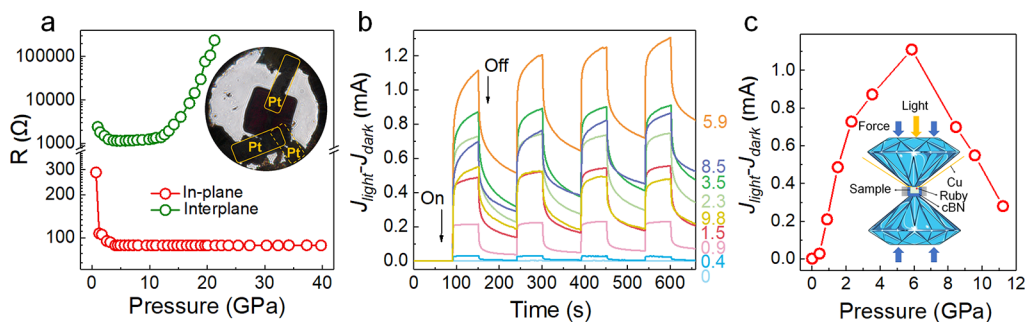


Figure 3. *In situ* resistance and photocurrent measurements under pressures. (a) Pressure-induced resistance evolution of single-crystal $\text{Bi}_2\text{O}_2\text{S}$. Both in-plane and interlayer resistances were recorded. (b) Photocurrents of $\text{Bi}_2\text{O}_2\text{S}$ during compression. (c) The photocurrent as a function of pressure. The inset shows a schematic illustration of the experimental setup within a DAC.

evolution can be ascribed to the suppression of the LPEs, i.e., that the strong nonlinear repulsive electrostatic force from $\text{Bi}6s^2$ LPEs resists the shrinkage of the $\text{Bi}\cdots\text{S}$ bond at pressures over 6.4 GPa. Surprisingly, at above 13.2 GPa, the $\text{Bi}\cdots\text{S}$ and $\text{Bi}-\text{O}$ bond distances exhibit a sudden downturn and upturn, respectively. Such an unusual phenomenon is related to the disappearance of the LPEs and the formation of the $\text{Bi}-\text{S}$ covalent bonds during compression, which results in a sudden shortening of the $\text{Bi}-\text{S}$ distances and stretch of the $\text{Bi}-\text{O}$ bond. Eventually, the disappearance of the LPEs induces a 2D-to-3D isostructural transition beyond 13.2 GPa, where all Bi valence electrons ($6s^26p^3$) involve bonding (Figure 1f).

Such a pressure-induced anomalous evolution of the lattice structures caused by the lone-pair electronic reconfiguration motivated us to uncover the LPE effects on the electronic and optoelectronic properties of $\text{Bi}_2\text{O}_2\text{S}$. We first traced the variation of the bandgap under high pressure using *in situ* UV–vis–NIR absorption spectroscopy. As shown in Figures 2 and S5, the band edge was determined to be 1.6 eV at ambient pressure, in line with a previous report.⁵ The bandgap increases from 1.6 to 1.9 eV during compression up to 18.0 GPa, accompanied by the color changing from black to red. A similar variation of bandgap has been found in BiOCl and $\text{Bi}_2\text{O}_2\text{Se}$ during compression.^{20,21} Such a blueshift of the bandgap is attributed to the pressure-induced weakening of the $\text{Bi}-6s$ states, as evidenced by the calculated electronic structures (Figure S6) where the suppression of LPEs pulls down the VB. Further compression from 18.0 to 39.5 GPa leads to the gradual decrease of the bandgap to 1.47 eV. The redshift is associated with the broadening of the VB caused by the shortening of the $\text{Bi}-\text{S}$ bond.^{22,23} The observation of the

irreversible bandgap evolution during compression–decompression cycles is owing to the irreversibility of the lone-pair stereochemical behavior in the structure (Figure 2c).

The electron transport property is another key parameter for optoelectronic materials. We performed *in situ* resistance measurements up to 40 GPa to explore the conductivity evolution of $\text{Bi}_2\text{O}_2\text{S}$ (Figure 3a). Considering the anisotropic feature of the layered $\text{Bi}_2\text{O}_2\text{S}$, we simultaneously measured the in-plane and interplane resistances of a single crystal with an obviously smaller in-plane resistance. During compression, the in-plane resistance decreases sharply and then remains nearly constant at above 5 GPa. In view of the multicomponent structure, electrons are more likely to transport along the conductive $\text{Bi}-\text{S}$ layers rather than the insulating $\text{Bi}-\text{O}$ layers.²⁴ Hence, the repulsion of the LPEs resists the shrinkage of the $\text{Bi}\cdots\text{S}$ bonds and, consequently, inhibits further resistance decreasing above 5 GPa. On the other hand, the interlayer resistance first decreases until 5 GPa is reached and then keeps almost constant up to 13 GPa. Thereafter, it shows an exponential increase, which is very different from the variation of the in-plane resistance. This variation of electron transport property is closely correlated to the 2D-to-3D structural changes, which are dominated by the dynamic stereochemical role of LPEs. The disappearance of the LPEs leads to a sudden rebound of the $\text{Bi}-\text{O}$ distances, which play a critical role in the exponential increase of resistance above 13 GPa.

Considering the promoted electron transport, it is presumable to expect enhanced optoelectronic property. To verify this, we conducted *in situ* photocurrent measurements. As shown in Figures 3b, 3c, and S7, the $\text{Bi}_2\text{O}_2\text{S}$ exhibits an

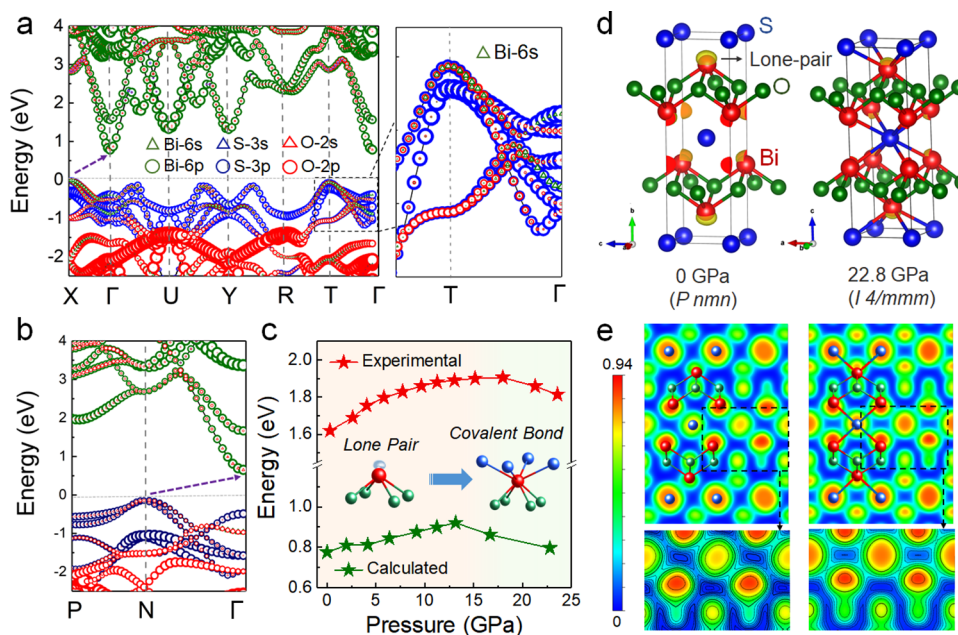


Figure 4. Pressure-induced variations of the electronic properties of $\text{Bi}_2\text{O}_2\text{S}$. Calculated band structures at (a) 0 and (b) 22.8 GPa. (c) The pressure dependency of bandgap derived from both UV–vis absorption spectroscopy and DFT calculations. (d) The ELF graph and (e) valence electron density map of $\text{Bi}_2\text{O}_2\text{S}$ at ambient pressure and 22.8 GPa. The ball-and-stick models with an isosurface value of 0.94 projects onto the (0 1 0) plane.

obvious photoresponse to visible light with an on–off switch ranging from 0 to 11.2 GPa. The photocurrent significantly grows with pressure and reaches the maximum value at 5.9 GPa, which is three orders of magnitude higher than the one at ambient pressure (Figure 3c). Owing to the highly distorted structure of the $\text{Bi}_2\text{O}_2\text{S}$ before the phase transition, the LPEs bring a high momentary polarizing field, which gives rise to efficient carrier transport and separation.^{12,25} Taken together, with the highest conductivity that resulted from the stereochemical role of LPEs, the considerably enhanced photocurrent is achieved around 5 GPa.

Intriguingly, these phenomena are contrary to our empirical cognition that the longer Bi–S bond should be easier to compress in the whole pressure region and that the bandgap should monotonously decrease during compression. The anomalously low compressibility between 5 to 13 GPa can be attributed to the stereochemical role of LPEs. To simulate the dynamic evolution of the LPEs under pressure in theory, we carried out DFT calculations on the electronic structures and electron localization function (ELF) (details in the Supporting Information). An indirect bandgap of ~ 0.77 eV was simulated at ambient pressure (Figure 4a). The variation tendency of the theoretical results is consistent with the bandgaps obtained from UV–vis–NIR absorption spectroscopy (Figure 4c). As shown in Figures 4a and S8, the Bi-6s and S-3p states mainly contribute to the valence band maximum (VBM) around the Γ point, while the conduction band minimum (CBM) mainly consists of the Bi-6p state with a minor contribution from the O-2s state. At 22.8 GPa, different from the situation at ambient pressure, the VBM around the Γ point in the partial band structure is mainly composed of O-2p and S-3p states (Figure 4b). This difference indicates the disappearance of the lone-pair Bi-6s² and the formation of Bi–S bonding under high pressure. Specifically, the energetic mismatch between the empty Bi-6p band and the Bi-6s/S-3p-based bands is gradually diminished because the dispersion of all bands becomes larger when Bi and S atoms move closer to

each other in the distorted structure.²⁶ Hence, the empty Bi-6p states become available for bonding S-3p valence orbitals to create a 3D structure of $\text{Bi}_2\text{O}_2\text{S}$ under high pressure.

The bonding nature of $\text{Bi}_2\text{O}_2\text{S}$ is signified by the sharing and localization of the valence electrons, which can be analyzed through the calculated ELF. The isosurface of a lobe-like charge extension around the Bi atom is the classic signature of the 6s² LPEs (Figure 4d), which possesses a relatively strong nonlinear repulsive electrostatic force between interlayers.²⁷ The LPEs around the Bi atoms are gradually suppressed and eventually disappear during compression. At 22.8 GPa, the ELF graph presents a negligible residual charge density of Bi-6s² LPEs in the tetragonal $\text{Bi}_2\text{O}_2\text{S}$ (Figure 4d), which confirms the 2D-to-3D structural transition. The ELF value lies by definition between 0 and 0.94, which was used to characterize the degree of electron localization and to quantitatively identify the character of the chemical bonds (details in the Supporting Information). The valence electron density map on the (0 1 0) surface presents lower charge distributions (ELF = 0.15 and 0.42 along two types of Bi–S bonds) at 0 GPa (Figure 4e), which indicates a weak Bi–S bonding. By contrast, at 22.8 GPa, the charge projection along the Bi–S direction suggests an enhanced bonding between Bi and the neighboring S atoms with ELF = 0.62 (Figure 4e), resulting in the formation of covalent bonds. In order to further verify the pressure-induced formation of Bi–S bonding experimentally, we collected *in situ* Raman spectra during compression and decompression (Figures S9 and S10 and detailed discussion in the Supporting Information). All Raman-active vibrations come from the Bi–O layers, without contributions from S atoms.^{28,29} Under high pressures, a new Raman peak appears at around 225 cm⁻¹ at 11.8 GPa, which comes from the vibrations of the Bi–S bonding.³⁰ This finding further confirms the formation of Bi–S bonding and the disappearance of LPEs.

In conclusion, using pressure engineering, we articulate the dynamic stereochemical role of LPEs on the crystal structures, electronic behaviors, and physical properties of a 2D bismuth

oxysulfide $\text{Bi}_2\text{O}_2\text{S}$. Through a comprehensive *in situ* high-pressure characterization combined with DFT calculations, we reveal the critical role of LPEs on the anomalous variations of structure and properties. The pressure-suppressed lone-pair effect of $\text{Bi}^{3+}\text{-}6s^2$ causes the weakening of phonon anharmonicity and Bi^{3+} centering, which contribute to an orthorhombic-to-tetragonal transition at 6.4 GPa. This phase transition effectively modulates the electrical and optoelectronic properties, leading to enhanced electron transport and a significant increase in photocurrent by three orders of magnitude. The strong nonlinear repulsive electrostatic force of LPEs during further compression resists the shrinkage of $\text{Bi}\cdots\text{S}$ bonds, resulting in abnormally low compressibility. In addition, optical measurements reveal an unusual blueshift of the bandgap associated with the gradually weakened stereochemical role of $\text{Bi}\text{-}6s^2$ LPEs. Above 13.2 GPa, the formation of $\text{Bi}\text{-S}$ bonding leads to a 2D-to-3D structural transition with the eventual disappearance of the LPEs. This work not only deepens our fundamental understanding of the stereochemical role of LPEs on structural and physical properties but also provides new insights into materials design by regulating the characters of lone pair stereochemistry.

■ ASSOCIATED CONTENT

Supporting Information

The Supporting Information is available free of charge at <https://pubs.acs.org/doi/10.1021/acs.jpcllett.0c02893>.

Experimental details, crystal structure details, SEM analysis, Raman analysis, supplementary equations, ELF, and DFT calculations of $\text{Bi}_2\text{O}_2\text{S}$ (PDF)

■ AUTHOR INFORMATION

Corresponding Author

Xujie Lü – Center for High Pressure Science and Technology Advanced Research (HPSTAR), Shanghai 201203, P. R. China; orcid.org/0000-0001-8402-7160; Email: xujie.lu@hpstar.ac.cn

Authors

Kejun Bu – Center for High Pressure Science and Technology Advanced Research (HPSTAR), Shanghai 201203, P. R. China

Hui Luo – Center for High Pressure Science and Technology Advanced Research (HPSTAR), Shanghai 201203, P. R. China

Songhao Guo – Center for High Pressure Science and Technology Advanced Research (HPSTAR), Shanghai 201203, P. R. China

Mei Li – Center for High Pressure Science and Technology Advanced Research (HPSTAR), Shanghai 201203, P. R. China

Dong Wang – Center for High Pressure Science and Technology Advanced Research (HPSTAR), Shanghai 201203, P. R. China; orcid.org/0000-0001-5004-9732

Hongliang Dong – Center for High Pressure Science and Technology Advanced Research (HPSTAR), Shanghai 201203, P. R. China

Yang Ding – Center for High Pressure Science and Technology Advanced Research (HPSTAR), Shanghai 201203, P. R. China

Wenge Yang – Center for High Pressure Science and Technology Advanced Research (HPSTAR), Shanghai 201203, P. R. China

Complete contact information is available at:

<https://pubs.acs.org/doi/10.1021/acs.jpcllett.0c02893>

Author Contributions

The manuscript was written through contributions of all authors. All authors have given approval to the final version of the manuscript.

Notes

The authors declare no competing financial interest.

■ ACKNOWLEDGMENTS

This work is supported by the National Nature Science Foundation of China (NSFC) (51527801 and U1530402). The high-pressure XRD measurements were performed at Sector 15 U of the Shanghai Synchrotron Radiation Facility (SSRF). The authors thank Xiaohuan Qi for her technique assistance with SEM experiments and appreciate the language editing by editor Freyja O'Toole.

■ REFERENCES

- (1) Liu, X.; Zhang, S.; Guo, S.; Cai, B.; Yang, S. A.; Shan, F.; Pumera, M.; Zeng, H. Advances of 2D Bismuth in Energy Sciences. *Chem. Soc. Rev.* **2020**, *49*, 263–285.
- (2) Zhao, L. D.; He, J.; Berardan, D.; Lin, Y.; Li, J. F.; Nan, C. W.; Drago, N. BiCuSeO Oxyselenides: New Promising Thermoelectric Materials. *Energy Environ. Sci.* **2014**, *7*, 2900–2924.
- (3) Zhang, K. L.; Liu, C. M.; Huang, F. Q.; Zheng, C.; Wang, W. D.; Study of the Electronic Structure and Photocatalytic Activity of the BiOCl Photocatalyst. *Appl. Catal., B* **2006**, *68*, 125–129.
- (4) An, H.; Du, Y.; Wang, T.; Wang, C.; Hao, W.; Zhang, J. Photocatalytic Properties of BiOX (X = Cl, Br, and I). *Rare Met.* **2008**, *27*, 243–250.
- (5) Zhang, X.; Liu, Y.; Zhang, G.; Wang, Y.; Zhang, H.; Huang, F. Q. Thermal Decomposition of Bismuth Oxysulfide from Photoelectric $\text{Bi}_2\text{O}_2\text{S}$ to Superconducting $\text{Bi}_4\text{O}_4\text{S}_3$. *ACS Appl. Mater. Interfaces* **2015**, *7*, 4442–4448.
- (6) Nguyen, S.; Yeon, J.; Kim, S.; Halasyamani, P. BiO(IO_3): A New Polar Iodate that Exhibits an Aurivillius-Type $(\text{Bi}_2\text{O}_2)^{2+}$ Layer and A Large SHG Response. *J. Am. Chem. Soc.* **2011**, *133*, 12422–12425.
- (7) Saha, S. Exploring the Origin of Ultralow Thermal Conductivity in Layered BiOCuSe. *Phys. Rev. B: Condens. Matter Mater. Phys.* **2015**, *92*, 041202.
- (8) Song, H. Y.; Ge, X. J.; Shang, M. Y.; Lü, J. T. Anharmonic Inter-Layer Bonding Leads to Intrinsically Low Thermal Conductivity of Bismuth Oxychalcogenides. *arXiv (Condensed Matter, Materials Science)*, January 6, **2019**, 1901.01490. <https://arxiv.org/abs/1901.01490> (accessed 2020).
- (9) Meng, S.; Zhang, X.; Zhang, G.; Wang, Y.; Zhang, H.; Huang, F. Synthesis, Crystal Structure, and Photoelectric Properties of A New Layered Bismuth Oxysulfide. *Inorg. Chem.* **2015**, *54*, 5768–5773.
- (10) Skoug, E.; Morelli, D. Role of Lone-Pair Electrons in Producing Minimum Thermal Conductivity in Nitrogen-Group Chalcogenide Compounds. *Phys. Rev. Lett.* **2011**, *107*, 1–5.
- (11) Nielsen, M.; Ozolins, V.; Heremans, J. Lone Pair Electrons Minimize Lattice Thermal Conductivity. *Energy Environ. Sci.* **2013**, *6*, 570–578.
- (12) Bu, K.; Luo, M.; Wang, R.; Zhang, X.; He, J.; Wang, D.; Zhao, W.; Huang, F. Q. Enhanced Photoelectric SrOCuSbS₂ of A [SrO]-Intercalated CuSbS₂ Structure. *Inorg. Chem.* **2019**, *58*, 69–72.
- (13) Zhang, G.; Wu, H.; Li, G.; Huang, Q.; Yang, C.; Huang, F.; Liao, F.; Lin, J. New High T_c Multiferroics KBiFe_2O_5 with Narrow Band Gap and Promising Photovoltaic Effect. *Sci. Rep.* **2013**, *3*, 1265.
- (14) Fabini, D. H.; Laurita, G.; Bechtel, J. S.; Stoumpos, C. C.; Evans, H. A.; Kontos, A. G.; Raptis, Y. S.; Falaras, P.; Van der Ven, A.; Kanatzidis, M. G.; Seshadri, R. Dynamic Stereochemical Activity of the Sn^{2+} Lone Pair in Perovskite CsSnBr_3 . *J. Am. Chem. Soc.* **2016**, *138*, 11820–11832.
- (15) Yang, W.; Huang, X.; Harder, R.; Clark, J. N.; Robinson, I. K.; Mao, H. K. Coherent Diffraction Imaging of Nanoscale Strain

Evolution in A Single Crystal under High Pressure. *Nat. Commun.* **2013**, *4*, 1680.

(16) Zeng, Q.; Sheng, H.; Ding, Y.; Wang, L.; Yang, W.; Jiang, J. Z.; Mao, W. L.; Mao, H. K. Long-Range Topological Order in Metallic Glass. *Science* **2011**, *332*, 1404–1406.

(17) Yoo, C. S. Chemistry under Extreme Conditions: Pressure Evolution of Chemical Bonding and Structure in Dense Solids. *Matter Radiat. at Extremes*. **2020**, *5*, 018202.

(18) Li, M.; Liu, T. B.; Wang, Y. G.; Yang, W. G.; Lü, X. J. Pressure Responses of Halide Perovskites with Various Compositions, Dimensionalities, and Morphologies. *Matter Radiat. at Extremes* **2020**, *5*, 018201.

(19) Wu, J.; Yuan, H.; Meng, M.; Chen, C.; Sun, Y.; Chen, Z.; Dang, W.; Tan, C.; Liu, Y.; Yin, J.; et al. High Electron Mobility and Quantum Oscillations in Non-Encapsulated Ultrathin Semiconducting Bi₂O₂Se. *Nat. Nanotechnol.* **2017**, *12*, 530–534.

(20) Zhao, J.; Xu, L.; Liu, Y.; Yu, Z.; Li, C.; Wang, Y.; Liu, Z. Isostructural Phase Transition in Bismuth Oxide Chloride Induced by Redistribution of Charge under High Pressure. *J. Phys. Chem. C* **2015**, *119*, 27657–27665.

(21) Pereira, A. L. J.; Santamaria-Perez, D.; Ruiz-Fuertes, J.; Manjon, F. J.; Cuenca-Gotor, V. P.; Vilaplana, R.; Gomis, O.; Popescu, C.; Munoz, A.; Rodriguez-Hernandez, P.; Segura, A.; Gracia, L.; Beltran, A.; Ruleova, P.; Drasar, C.; Sans, J. A. Experimental and Theoretical Study of Bi₂O₂Se under Compression. *J. Phys. Chem. C* **2018**, *122*, 8853–8867.

(22) Chouinard, C.; Desgreniers, S. Bi₂O₃ under Hydrostatic Pressure: Observation of A Pressure-Induced Amorphization. *Solid State Commun.* **1999**, *113*, 125–129.

(23) Zhang, G.; Zhang, Q.; Hu, Q.; Wang, B.; Yang, W. Giant Enhancements in Electronic Transport and Photoelectric Properties of Bismuth Oxysulfide by Pressure-Driven 2D-3D Structural Reconstruction. *J. Mater. Chem. A* **2019**, *7*, 4019–4025.

(24) Bu, K. J.; Huang, J.; Luo, M.; Guan, M.; Zheng, C.; Pan, J.; Zhang, X.; Wang, S.; Zhao, W.; Shi, X.; Xu, L.; Huang, F. Q. Observation of High Seebeck Coefficient and Low Thermal Conductivity in [SrO]-Intercalated CuSbSe₂ Compound. *Chem. Mater.* **2018**, *30*, 5539–5543.

(25) Remsing, R.; Klein, M. Lone Pair Rotational Dynamics in Solids. *Phys. Rev. Lett.* **2020**, *124*, 066001.

(26) Häussermann, U.; Berastegui, P.; Carlson, S.; Haines, J.; Léger, J. M. TlF and PbO under High Pressure: Unexpected Persistence of the Stereochemically Active Electron Pair. *Angew. Chem.* **2001**, *113*, 4760–4765.

(27) Feng, Z.; Jia, T.; Zhang, J.; Wang, Y.; Zhang, Y. Dual Effects of Lone-Pair Electrons and Rattling Atoms in CuBiS₂ on Its Ultralow Thermal Conductivity. *Phys. Rev. B: Condens. Matter Mater. Phys.* **2017**, *96*, 235205.

(28) Cheng, T.; Tan, C.; Zhang, S.; Tu, T.; Peng, H.; Liu, Z. Raman Spectra and Strain Effects in Bismuth Oxychalcogenides. *J. Phys. Chem. C* **2018**, *122*, 19970–19980.

(29) Xu, Y. D.; Wang, C.; Lv, Y. Y.; Chen, Y.; Yao, S. H.; Zhou, J. Infrared and Raman Spectra of Bi₂O₂X and Bi₂OX₂ (X= S, Se, and Te) Studied from First Principles Calculations. *RSC Adv.* **2019**, *9*, 18042–18049.

(30) Efthimiopoulos, I.; Kemichick, J.; Zhou, X.; Khare, S. V.; Ikuta, D.; Wang, Y. High-Pressure Studies of Bi₂S₃. *J. Phys. Chem. A* **2014**, *118*, 1713–1720.